PCCP

ROYAL SOCIETY OF CHEMISTRY

PAPER

View Article Online
View Journal | View Issue

Cite this: *Phys. Chem. Chem. Phys.*, 2025, **27**, 7004

Measurement of carbon monoxide pressure broadening and temperature dependence coefficients in the 1 ← 0 band

Denghao Zhu, †*[a] Leopold Seifert,[a] Sumit Agarwal,[a] Bo Shu,[a] Ravi Fernandes[ab] and Zhechao Qu *[a]

Two laser absorption spectroscopy (LAS)-based spectrometers have been developed for measuring carbon monoxide (CO) pressure broadening and temperature dependency coefficients in the 1 ← 0 band. Using a scanned-wavelength LAS at 140 Hz, pressure broadening coefficients of four CO transition lines P(16), P(20), P(26), and P(27), perturbed by Ar, He, H_2, O_2, N_2, CO_2, and Air have been systematically measured in a gas cell using a consistent metrological approach. Results indicate that the CO pressure broadening coefficient decreases monotonically as the line number $|m|$ increases. The variation of pressure broadening coefficients at different buffer gases follow a consistent trend for all four measured lines: CO–H_2 and CO–Ar show the highest and lowest pressure broadening coefficients, respectively. Compared to the literature results with relatively large uncertainties or even unavaible uncertainty information, the uncertainty of measured pressure broadening coefficients is below 1% for most cases. Further, using a scanned-wavelength LAS at 20 kHz, temperature dependence coefficients of P(20) in Ar, He, N_2 and CO_2 were measured at a temperature range of 430–1648 K in a shock tube. With this rapid scan frequency, the spectrum between incident shock and reflected shock was also used for temperature dependence coefficient calculation. The uncertainty of the measured temperature dependence coefficients are under 6.2%. Toward combustion systems as an application case, the CO mole fraction during CH_4 oxidation in the shock tube was quantified using a fixed-wavelength LAS. The results reveal that the uncertainty in CO mole fraction was reduced by a factor of 2.7 when using the line parameters obtained in this study compared to those from the HITRAN database. Thus, the newly measured data with low uncertainties substantially enhance the spectroscopic database, enabling more precise CO mole fraction quantification across a range of application scenarios such as environmental monitoring, industrial control, safety monitoring, medicine, astronomy, and scientific research.

Received 13th January 2025,
Accepted 17th March 2025

DOI: 10.1039/d5cp00161g

rsc.li/pccp

1. Introduction

Carbon monoxide (CO) is a highly significant molecule utilized across various domains, including industry, environmental monitoring, astronomical research, and combustion studies. In industry, CO serves as a crucial feedstock to produce important chemicals such as methanol and acetic acid. Additionally, CO plays a vital role in metal refining, particularly in iron and steel production, where it acts as a reducing agent in blast furnaces to extract iron from its ore sources.[1,2] From an environmental perspective, CO is a major air pollutant, primarily generated by the incomplete combustion of fossil fuels. Although it is not a direct greenhouse gas, the oxidation of CO by hydroxyl radicals (OH) leads to the formation of ozone and carbon dioxide (CO_2), thereby contributing indirectly to climate change.[3–5] In the field of astronomy, CO is one of the most abundant molecules in space. It is commonly used to trace molecular clouds in the interstellar medium, providing critical insights into star formation and galactic evolution.[6–8] CO is a key intermediate in combustion studies. Understanding its formation and behavior is essential for optimizing combustion efficiency and reducing harmful emissions.[9–11] From a safety standpoint, CO is highly toxic to humans because it binds to hemoglobin more effectively than oxygen, resulting in carbon monoxide poisoning. It is also a major component of smoke produced in house fires, presenting a significant risk of poisoning during such events[12].

Concerning such broad application scenarios, accurate quantification of CO mole fraction becomes vital.

[a] *Department of Physical Chemistry, Physikalisch-Technische Bundesanstalt, Braunschweig, Germany. E-mail: denghao.zhu@seu.edu.cn, zhechao.qu@ptb.de*
[b] *Institute of Internal Combustion Engines, Technische Universität Braunschweig, Braunschweig, Germany*
† Current address: School of Energy and Environment, Southeast University, Nanjing, China.

Laser absorption spectroscopy (LAS) is an advanced *in situ*, non-invasive, and highly selective optical diagnostic technique that has been extensively developed and widely utilized for precise molecule fingerprint detection in various scientific and industrial applications. Several specific spectroscopic sensing techniques fall under the umbrella of LAS, each with its own advantages and applications. Direct absorption spectroscopy (DAS) is the most straightforward approach, where the attenuation of laser light due to molecular absorption is directly measured to determine species concentration and temperature. Wavelength modulation spectroscopy (WMS) enhances sensitivity by modulating the laser wavelength and detecting absorption signals at higher harmonics, making it particularly effective for low-concentration measurements in noisy environments. Off-axis integrated cavity output spectroscopy (OA-ICOS) combines the principles of cavity-enhanced spectroscopy with off-axis alignment to achieve highly sensitive and precise measurements of gas-phase species. The dual-comb spectroscopy technique leverages the interference of two frequency combs to achieve ultra-high spectral resolution and rapid data acquisition, enabling the simultaneous detection of multiple species with exceptional precision. Photoacoustic spectroscopy (PAS), on the other hand, detects acoustic waves generated by the absorption of modulated laser light, offering high sensitivity and suitability for trace gas analysis. These techniques have been extensively validated and applied in a wide range of fields, as evidenced by numerous studies.[13–17]

To implement LAS, accurate spectroscopic parameters are the premise. CO has a strong characteristic absorption band in the infrared (IR) region. The most prominent IR band of CO is centered around 4.7 μm, corresponding to the transition from the ground vibrational state (v = 0) to the first excited vibrational state (v = 1). The first overtone band of CO (Δv = 2) is near 2.3 μm and the second overtone band (Δv = 3) is near 1.55 μm. The line intensity of the fundamental band is approximately 10 000 and 100 times stronger compared to the overtone bands near 1.55 μm and 2.3 μm, respectively.[18] Besides, the fundamental band has relatively weaker interference from common species, making it more promising for sensitive detection.

For decades, spectroscopic parameters of CO in the 1 ← 0 band have been extensively studied.[19–31] With the development of optical techniques and molecule spectroscopy theory, the quantity and accuracy of the spectroscopic data are continuously improving. Nevertheless, there are still some spaces that need to be improved. Firstly, most pressure broadening coefficients were measured using air as the buffer gas. For example, in the HITRAN database,[32] broadening parameters due to pressure of ''planetary'' (H_2, CO_2, He) gases were only introduced in 2016 and most data were generated from extrapolating very limited experimental data. Broadening parameters in other buffer gases are scarce. In some specific applications, such as combustion study, Ar, He and N_2 are commonly used buffer gases. The relevant spectroscopic data becomes vital. Therefore, systematic spectroscopic parameters at a variety of buffer gases are required. Secondly, most studies report the line parameters of CO with a line number $|m|$ below 25. However, at elevated temperatures, higher rotational levels will be significantly populated. To complement the entire database, more efforts should be made to the absorption lines with higher $|m|$. Thirdly, compared to pressure broadening coefficients, there is much less data available for temperature dependence coefficients. One of the main reasons is a higher requirement for experimental facilities. Fourier-transform infrared spectroscopy (FTIR) is the most used, and the working temperature is generally below 296 K. Using a heated cell can target higher temperatures but typically below 1000 K. To achieve even higher temperatures, a shock tube is considered an ideal reactor that can create a quasi-instantaneously and homogeneously high temperature and pressure environment with a time scale of microseconds or milliseconds. Most spectroscopic measurements for combustion or space exploration studies were done in a shock tube. For example, for line P(20) investigated in this study, Ren *et al.*,[18] Spearrin *et al.*[33] and Grégoire *et al.*[34] measured temperature dependence coefficients in a shock tube.

In this study, the focus is to measure the pressure broadening and temperature dependence coefficients of four specific CO transitions near 4.9 μm: P(16), P(20), P(26), and P(27). Two in-house spectrometers have been built accordingly. Specifically, a scanned-wavelength LAS operating at 140 Hz was used to measure the pressure broadening coefficients of those four CO transition lines perturbed by Ar, He, H_2, O_2, N_2, CO_2, and air in a gas cell. Then, the temperature dependence coefficients of P(20) in Ar, He, N_2 and CO_2 were measured in a shock tube using a scanned-wavelength LAS at 20 kHz. This much faster scan frequency compared to pressure broadening measurements is to match the short timescale of shock tube processes. As an application case, the time-resolved CO mole fraction during CH_4 oxidation in the shock tube was measured using a fixed-wavelength LAS. The uncertainty of CO mole fraction has been metrologically analysed and compared based on the line parameters measured in this study and from HITRAN.

2. Methodology

To accurately quantify the foreign pressure broadening and temperature dependence coefficients, the widely used technique, laser absorption spectroscopy (LAS), has been employed. For LAS, the transmitted intensity $I_t(\upsilon)$ of a monochromatic laser source through a gaseous sample is given by Beer–Lambert law:[17]

$$I_t(\upsilon) = E(t) + I_0(\upsilon)\cdot\eta(t)\cdot\exp[-\alpha(\nu)] \quad (1)$$

with the background emission $E(t)$ at time t, initial laser intensity $I_0(\upsilon)$, absorbance $\alpha(\nu)$, and the broadband transmission losses $\eta(t)$, which are synchronously derived from the individual raw signals and absorption profiles. The exponential term can be computed using the following equation:

$$\alpha(\nu) = -\ln\left(\frac{I_t(\nu) - E(t)}{I_0(\nu)\cdot\eta(t)}\right) \quad (2)$$

The Voigt function can be used to model the line shape of the absorbance spectrum in eqn (2), which considers the

combined effects of Doppler and collisional broadening on the spectral line. These effects are characterized by the Doppler broadening full width at half maximum (FWHM), $\Delta\nu_D$, and the collisional-broadening FWHM, $\Delta\nu_L$, given by

$$\Delta\nu_D = \nu_0\sqrt{\frac{8k_B T \ln 2}{Mc^2}} \quad (3)$$

$$\Delta\nu_L = 2\cdot p\cdot\left(\frac{T_0}{T}\right)^n\cdot[\gamma_s\cdot x+\gamma_f\cdot(1-x)] \quad (4)$$

where ν_0 is the center wavelength, k_B is the Boltzmann constant with a value of 1.380649×10^{-23} J K^{-1}, T is the temperature, M is the molecular mass of the absorbing species, c is the speed of light, p is the total pressure, x is the mole fraction of CO, γ_s and γ_f are the self and foreign broadening coefficients, T_0 is the reference temperature of 296 K, n is the temperature dependence coefficient. In this study, the contribution of self-broadening is negligible with a low CO mole fraction. Therefore, the eqn (4) can be transformed into:

$$\ln\left(\frac{\Delta\nu_L}{2\cdot p}\right) = n\cdot\ln\left(\frac{T_0}{T}\right)+\ln(\gamma_f\cdot(1-x)) \quad (5)$$

The temperature dependence coefficient can be obtained from the slope of the linear regression between $\ln\left(\frac{\Delta\nu_L}{2\cdot p}\right)$ and $\ln\left(\frac{T_0}{T}\right)$.

3. Experimental setup

To measure the pressure broadening and temperature dependence coefficient, two in-house LAS-based spectrometers have been established. The schematic of these two experimental setups is shown in Fig. 1. Pressure broadening coefficient measurement, as shown in Fig. 1(a), is a static measurement conducted in a gas cell. Two CO lasers were used to target four transitions. A continuous-wave distributed-feedback interband cascade laser (CW-DFB-ICL, Nanoplus) centered at 4855 nm (2059.7 cm^{-1}) was used to study the CO transition P(20). Another CW-DFB-ICL (Nanoplus) centered at 4925 nm (2030.4 cm^{-1}) can cover CO transitions of P(27), P(16) and P(26). The laser wavelength was tuned by a laser diode controller (PRO8000 equipped with LDC8002 and TED8020, Thorlabs) together with a function generator (KEYSIGHT, 33500B). The tuning frequency was set as 140 Hz with a triangle-shaped current ramp. The dynamic laser tuning was determined before starting the measurements using a Germanium etalon (length 76.244 mm, traceable to PTB's (Physikalisch-Technische Bundesanstalt) length standard). The results of the etalon measurement were used to convert the x-axis of the measured spectra from the time to the wavenumbers domain. Both lasers were collimated into a 32.52 cm gas cell made of stainless steel and equipped with wedged CaF_2 windows. The lasers went through the sample gas and were divided into two branches by a beamsplitter and received by two detectors (PVI-4TE-5, VIGO). The signal was sampled with 16-bit resolution at

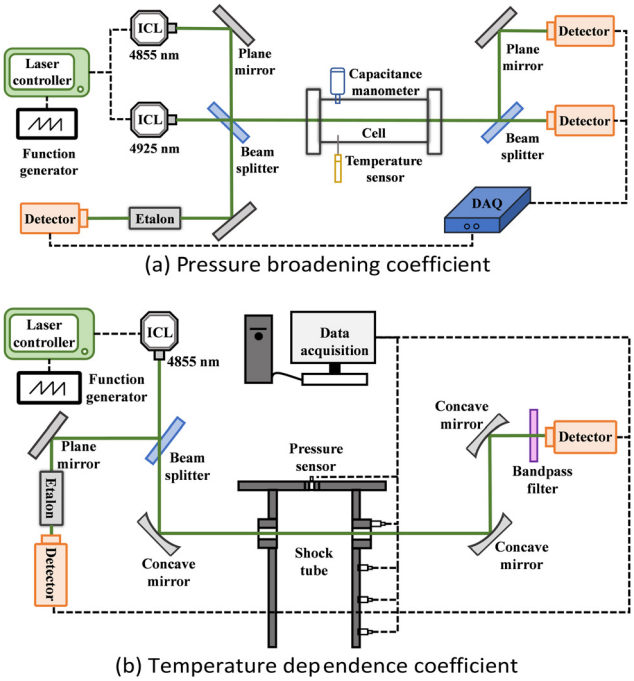

Fig. 1 Schematic of the experimental setup.

600 kHz by a data acquisition card (USB-6363, National Instruments). A capacitance manometer (0–1000 mbar, MKS Baratron) and a Pt100 thermocouple were used to measure gas pressure and temperature, respectively. Both sensors have been calibrated and were traceable to the SI using PTB's national pressure and temperature standards.

For temperature dependence coefficient measurement, a shock tube was used. A detailed description of the shock tube can be found in our previous paper,[35–37] so only a brief introduction is given here. The shock tube consists of a 3.5-meter driver section and a 4.5-meter driven section with an overall inner diameter of 7 cm. Five pressure sensors (603CAB, Kistler) were utilized for pressure measurements. The initial pressure (P_1) of the mixture charged into the driven section was measured by a pressure sensor (MKS Baratron, 0–1000 mbar). The pressure (P_2) and temperature (T_2) after the incident shock wave and the pressure (P_5) and temperature (T_5) after the reflected shock wave were calculated using the one-dimensional shock equations. For this study, only the temperature dependence coefficient of P(20) was measured which has been proven to be well suited for combustion-related study.[18]

Fig. 1(b) shows the established spectrometer for temperature dependence coefficient measurement by coupling LAS to the shock tube. As the time scale in the shock tube is in micro to milliseconds, the scan frequency of the laser was enhanced to 20 kHz for dynamic measurements. The laser beam was focused using a concave mirror (CM508-200-M01, 200 mm focal length, Thorlabs) and passed through optical windows positioned in the same plane as the fourth pressure sensor, with an optical path length of 7 cm. A separate laser branch was directed to the etalon and the signal was recorded prior to the measurements. After passing the gases, the laser was

focused onto a photodetector (PVI-4TE-5, VIGO) by a concave mirror (CM508-050-M01, focal length: 50 mm, Thorlabs). A narrow bandpass filter (CWL = 4856 nm, BW = 30 nm, laser components) was placed in front of the detector to separate the signal from the background emission $E(t)$ in eqn (1), *e.g.*, thermal emission from the shock-heated gases. The pressure and photodetector signals were recorded by a 16-bit 80 MS s^{-1} data acquisition card (M2p.5943-x4, Spectrum Instrumentation).

4. Results and discussions

4.1 Pressure broadening coefficients

Two lasers were used for pressure broadening coefficients of four CO transitions. The wavenumber and line intensity of these four lines are shown in Fig. 2 according to the HITRAN database. The laser centered at 4925 nm was used for P(27), P(16) and P(26) pressure broadening coefficients measurement. And the laser centered at 4855 nm was used for P(20) pressure broadening coefficients measurement.

To derive the foreign broadening coefficients, a high-quality pure CO (purity 5.0, Linde) was utilized. The procedure employed for gas mixture preparation is as follows: (1) evacuate the whole system including gas cell and all components in the gas manifold up to the gas cylinder; (2) flush the gas cell with pure CO and then evacuate the system; (3) repeat step 2 for three times; (4) keep pure CO in cell with a pressure below 0.5 mbar; (5) fill the buffer gas to a certain pressure and start the measurement over minutes; (6) partially evacuate the mixture to another certain pressure and record the data; (7) repeat step 6 at different pressures and buffer gases (Ar, He, H_2, O_2, N_2, CO_2 and air). The gas pressure in the cell was regulated by the gas cell outlet valve and the exhaust pump.

Fig. 3 shows an exemplary raw laser signal and an etalon signal in a half period, where a clearly isolated CO absorption peak can be observed. From the etalon signal, there is a non-uniform distribution of the peak's interval, indicating the non-linear behavior of the laser during the current modulation. The free spectral range (FSR) is calculated to be 0.01633 cm^{-1} at the center wavelength of 2059.91 cm^{-1} with a refractive index of 4.0167. With this information, it can convert the raw laser signal from the time-domain to frequency-domain.

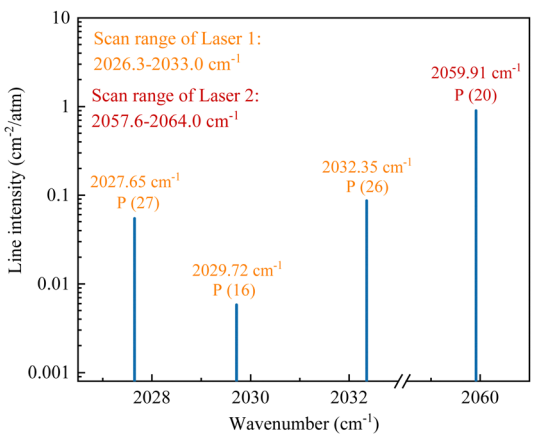

Fig. 2 CO transitions measured in this study.

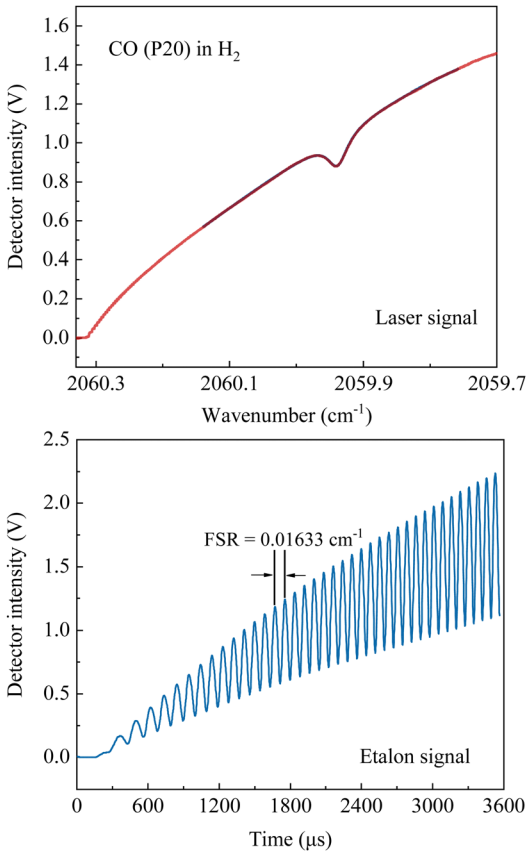

Fig. 3 Raw data of laser signal and etalon signal measured in the gas cell.

Because of a consistent procedure being used for different CO transitions as well as different buffer gases, only CO–H_2 broadening coefficient of P(20) line is illustrated as an example. Firstly, the measured laser signal was averaged over ten scans and fitted with a third-order polynomial for the baseline. It was converted to absorbance using Beer–Lambert raw according to eqn (1) and (2), as shown in Fig. 4(a). The absorption profile was fitted by the Voigt profile using a non-linear Levenberg–Marquart algorithm. The residual between measured and fitted data shown below in Fig. 4(a) is (1σ) 1.51×10^{-3} optical density. To clearly discriminate the pressure-broadening effect, the Gaussian width was calculated using the measured gas temperature according to eqn (3). The line width progression at different pressures was used to extract the pressure broadening coefficient. A weighted linear fit method (York Fit) was used to consider both the uncertainties from x and y axis. The pressure measurements were associated with 0.1–0.5% uncertainty (k = 1) according to PTB's pressure standard, of which the uncertainty has been considered for the linear regression as the x-error bar. The standard deviation (1σ) of the line width results (more than 200 measurements) at each pressure step, together with the wavenumber scale (laser tuning) uncertainty, was used as the y-error bar. Fig. 4(b) illustrates the linear regression between the Lorentzian FWHM and the pressure of CO–H_2,

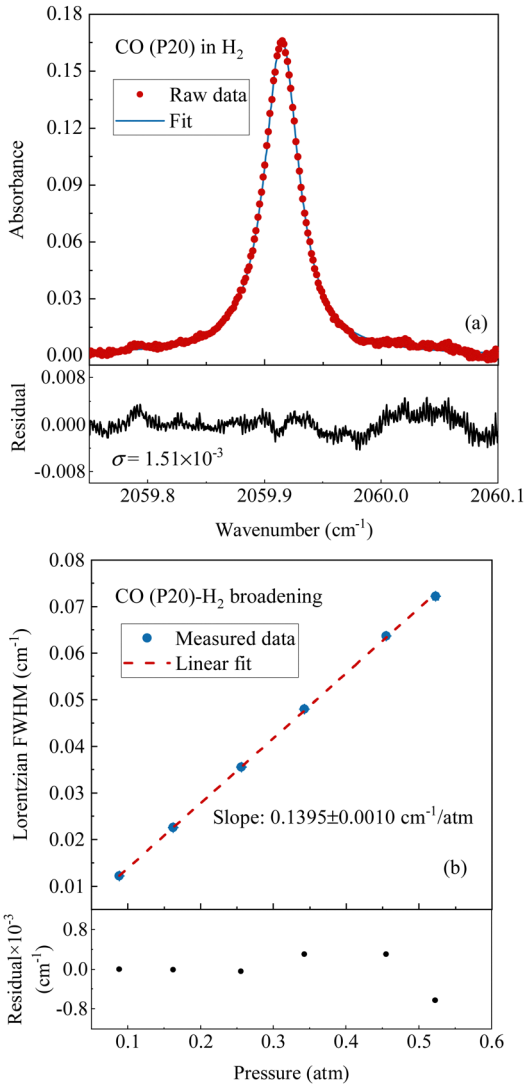

Fig. 4 (a) CO absorption spectrum of P(20) in H_2; (b) CO–H_2 pressure broadening of P(20) (the *x* and *y* axis error bars are hidden within the symbol).

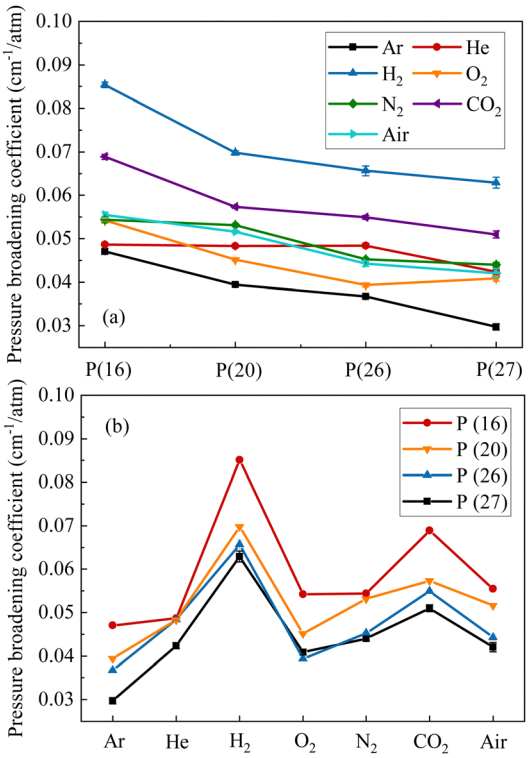

Fig. 5 (a) Pressure broadening coefficients *versus* line numbers; (b) pressure broadening coefficients *versus* buffer gases (the error bars are hidden within the symbol).

demonstrating excellent linearity. The residuals between measured data and linear fit are within 8×10^{-4} cm^{-1} range. The slope of the linear fit divided by 2 is the CO–H_2 broadening coefficient which is 0.06975 cm^{-1} per atm with an uncertainty of 0.0005 cm^{-1} per atm.

Following the same methodology, the pressure broadening coefficients at different buffer gases and for different CO transitions have been consistently measured and are shown in Fig. 5. From the results of the literature, the pressure broadening coefficient of CO monotonically decreases with the increase of line number $|m|$.[30] Our measured results also follow this tendency, namely pressure broadening coefficients decrease from P(16) ($m = -16$) to P(27) ($m = -27$). The variations of pressure broadening coefficients at different buffer gases are also well-aligned for four lines, *e.g.* the CO–H_2 and CO–Ar show the highest and lowest pressure broadening coefficients, respectively.

For those four specific CO absorption lines, some data is available in the literature and in the HITRAN database. Fig. 6 shows the comparison of pressure broadening coefficients between this study and the literature results. As mentioned in the Introduction part, most studies only report the results with $|m|$ below 25. Fig. 6 shows some literature data for P(16) and P(20) but very rare data for P(26) and P(27). Overall, our measured data align well with the literature results regarding the variation tendency of different buffer gases. The values are also aligned with some of the literature values and most values from HITRAN database. It is worth mentioning that for P(20), Crane-Robinson and Thompson[19] measured the pressure broadening over a variety of buffer gases, including Ar, He, H_2, O_2, N_2 and CO_2, using a grating spectrometer with a resolution of 0.1 cm^{-1}. Their results align well with the results of the literature and our measurements regarding the variation tendency, while the absolute values are lower overall and without uncertainty information (c.f. Table 1). This might be caused by the limited resolution and precision of the optical techniques at that time.

Table 1 summarizes the values of pressure broadening coefficients from the literature review and this study. Values in brackets denote uncertainties. As can be seen, none of the literature data provides systematic pressure broadening coefficient datasets of those four lines perturbed by those seven buffer gases (Ar, He, H_2, O_2, N_2, CO_2 and Air). Moreover, most literature results did not provide any information on uncertainties, or the uncertainties are much larger than the current study.

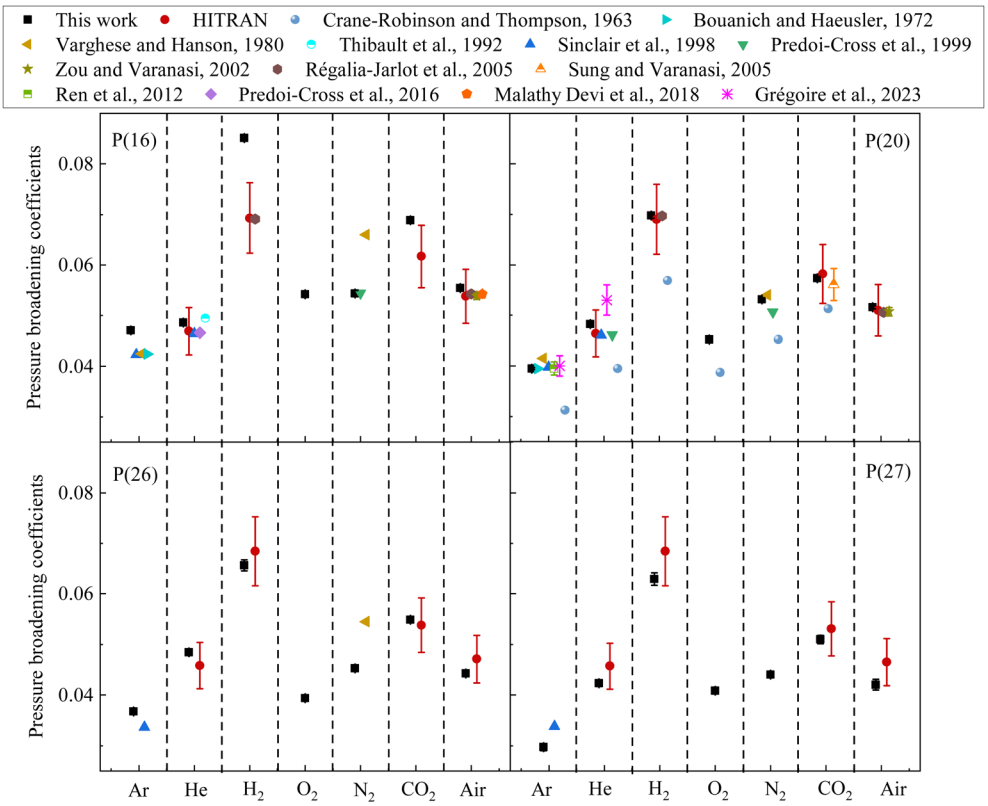

Fig. 6 Comparison of pressure broadening coefficients with literature results (the error bars are hidden within the symbol).

For example, the uncertainties from HITRAN database are 5–10%, while in this study, most uncertainties are less than 1%. Hence, the consistent experimental data provided in this study are valuable for CO mole fraction quantification. On the other hand, for CO–Air pressure broadening coefficients, it is also feasible to estimate it by combining CO–O_2 and CO–N_2 broadening coefficients with a proportion of $N_2 : O_2 = 79 : 21$ based on the binary collision approximation. The calculated CO-Air pressure broadening coefficients of P(16), P(20), P(26) and P(27) are 0.05432 0.05147 0.04401 0.04335, respectively. They are close to the directly measured CO-air pressure broadening coefficients with a disparity of 2.06%, 0.23%, 0.54%, 3.14%, respectively, underscoring the reasonability of the measurements.

4.2 Temperature dependence coefficients

Apart from pressure, temperature is also a key parameter that influences the line shape. To achieve a temperature above 1000 K, we used a shock tube as the heater. The pressure and temperature rise process in the shock tube is within microseconds. To meet the high demand of time-resolution, the laser tunning frequency was enhanced to 20 kHz. The temperature dependence coefficient of P(20) in four commonly used buffer gases for combustion study, including Ar, He, N_2 and CO_2 have been consistently measured in the shock tube. As already been illustrated in ref. 18 and 34, CO requires a significant time to be vibrationally relaxed behind the reflected shock wave, a small portion of H2 (1%) has been added to the 1% CO/98% Ar, 1% CO/98% N_2 and 1% CO/98% CO_2 mixtures. Helium itself has a strong effect on reducing vibrational relaxation time. From the simulation results by Grégoire *et al.*,[34] adding 20% He into CO/Ar mixture can already realize a shorter vibrational relaxation time than adding 1% H_2 into the mixture. Therefore, a 1% CO/99% He mixture was used to study CO–He temperature dependence coefficient without adding H_2.

Fig. 7 shows the raw laser signal, etalon signal and pressure of 1% CO/1% H_2/98% Ar mixture measured in the shock tube. The pressure was measured by the fourth sensor, which is located on the same plane as the laser. In the pressure profile, two sharp pressure rises can be distinguished, indicating the arrival of incident shock and reflected shock, respectively. For this case, the initial pressure (P_1) of the mixture is 0.04 bar. Then, the mixture was heated to 837 K and 0.31 bar by the incident shock wave and again heated to 1543 K and 1.20 bar by the reflected shock wave within 80 μs. Because of a highly diluted mixture being used, the pressure drop is negligible within a certain period.

For the laser signal, the line shape significantly changes during the shock propagation. When the incident and reflected shock pass through the optical window, two interferences can be observed in the laser signal caused by the Schlieren effect. Notably, in the previous literature work,[18,34] the scan frequency was limited to 2.5 kHz, and therefore only the spectrum at (T_5, P_5) was used. With the rapid scan frequency of 20 kHz used in this study, the spectrum at (T_2, P_2) was also used for the first time. This novel idea fulfils the feature of a shock tube that can get double information of two temperature and pressure

Table 1 Summary of pressure broadening coefficients of P(16), P(20), P(26) and P(27)

	Ar	He	H_2	O_2	N_2	CO_2	Air
P(16)							
1972, Bouanich and Haeusler[20]	0.04240						
1980, Varghese and Hanson[21]	0.04250				0.06600		
1992, Thibault *et al.*[22]		0.04950					
1998, Sinclair *et al.*[23]	0.04228	0.04647					
1999, Predoi-Cross *et al.*[24]					0.05447		
2002, Zou and Varanasi[25]							0.05380 (61)
2005, Régalia-Jarlot *et al.*[27]			0.06910				0.05430
2016, Predoi-Cross *et al.*[29]		0.04658					
2018, Devi *et al.*[30]							0.05419 (20)
HITRAN[32]		0.04690 (469)	0.06930 (693)			0.06170 (617)	0.05380 (538)
This study	0.04704 (61)	0.04864 (38)	0.08510 (61)	0.05423 (41)	0.05435 (65)	0.06889 (58)	0.05546 (59)
P(20)							
1963, Crane-Robinson *et al.*[19]	0.03120	0.03950	0.05690	0.03870	0.04520	0.05130	
1972, Bouanich and Haeusler[20]	0.03950						
1980, Varghese and Hanson[21]	0.04150				0.05400		
1998, Sinclair *et al.*[23]	0.03978	0.04605					
1999, Predoi-Cross *et al.*[24]		0.04615			0.05063		
2002, Zou and Varanasi[25]							0.05070 (79)
2005, Régalia-Jarlot *et al.*[27]			0.06970				0.05060
2005, Sung and Varanasi[28]							0.05610 (321)
2012, Ren *et al.*[18]	0.03950						
2023, Grégoire *et al.*[34]	0.04000	0.05300					
HITRAN[32]		0.04640 (464)	0.06900 (69)			0.05820 (582)	0.05100 (510)
This study	0.03947 (20)	0.04828 (32)	0.06977 (52)	0.04519 (6)	0.05314 (31)	0.05731 (32)	0.05159 (32)
P(26)							
1980, Varghese and Hanson[21]					0.05450		
1998, Sinclair *et al.*[23]	0.03363						
HITRAN[32]		0.04580 (458)	0.06840 (684)			0.05380 (538)	0.04710 (471)
This study	0.03676 (38)	0.04843 (52)	0.06564 (108)	0.03936 (46)	0.04524 (32)	0.05492 (42)	0.04425 (63)
P(27)							
1998, Sinclair *et al.*[23]	0.03379						
HITRAN[32]		0.04570 (457)	0.06840 (684)			0.05310 (531)	0.04650 (465)
This study	0.02973 (71)	0.04235 (69)	0.06288 (125)	0.04087 (63)	0.04401 (54)	0.05099 (81)	0.04203 (105)

The uncertainties are given in parentheses.

combinations within a single shot. Based on that, the temperature range covers from 430–1648 K and pressure ranges from 0.17–2.23 bar. On top of Fig. 7 is the measured etalon signal at 20 kHz to convert the laser signal from time-domain to frequency-domain.

The raw laser signal in a half period was extracted and fitted with a third-order polynomial for the baseline. Then the CO absorption profile can be obtained according to eqn (1) and (2). Fig. 8 shows the fitted baseline (reference signal), CO laser signals and absorbances at three stages during the shock propagation, where the effect of both pressure and temperature on the line shape can be clearly observed. For example, the absorption profile is significantly broadened at P_5 compared to P_1 and P_2. The absorbance at T_2 is the highest, which is reasonable according to the line intensity variation against the temperature of P(20), as shown in Fig. 10.

Further, the CO absorption spectrum was fitted by the Voigt profile using a non-linear Levenberg–Marquart algorithm, as shown in Fig. 9(a). Here the CO absorption profile at (T_5, P_5) is taken as an example. The residual between measured and fitted data is (1σ) 7.1×10^{-3} optical density. According to eqn (5), the line width progression at different temperatures was used to extract the temperature dependence coefficient. According to our previous study,[37] the uncertainties of T_2, T_5, P_2 and P_5 are 1.35%, 1.8%, 2% and 2.8% (k = 1), respectively. Those uncertainties have been considered as the x and y-error bar for linear regression. Fig. 9(b) shows the linear regression for CO–Ar temperature dependence. The slope of the linear fit is the CO–Ar temperature dependence coefficient which is 0.60484 with an uncertainty of 0.03701. As mentioned above, 1% H_2 has been added to the mixture considering the vibrational relaxation effect. We have also measured 1% CO/99% Ar mixture as a comparison. The temperature dependence coefficient of 1% CO/99% Ar mixture is 0.595, which is very close to that of 1% CO/1% H_2/98% Ar mixture. The detailed discussion on this part has beyond the scope of the current study, while the effect of vibrational relaxation on temperature dependence coefficients merit further investigations in the future.

Using the same method, temperature dependence coefficient of CO–He, CO–N_2 and CO–CO_2 of P(20) have been measured. Fig. 11 compares measured temperature dependency coefficients with results from the literature. The values are summarized in Table 2, of which the values in brackets denote uncertainties. From Fig. 11, the current results align with most

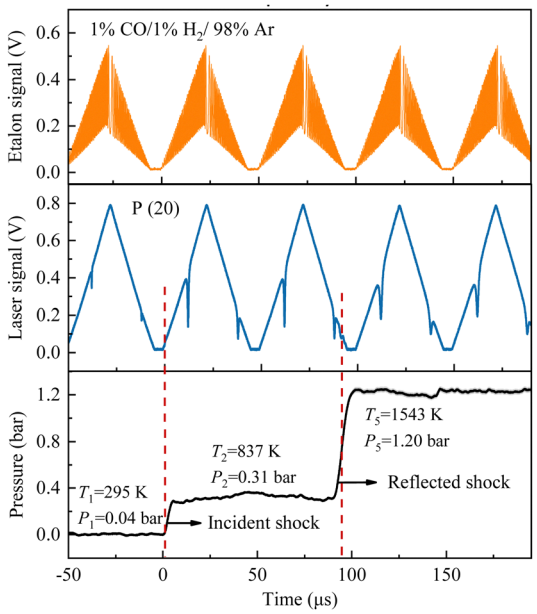

Fig. 7 Raw data of laser signal, etalon signal, and pressure measured in the shock tube.

literature results when taking uncertainties into account. This study is the first time to systematically measure the CO–Ar, CO–He, CO–N_2 and CO–CO_2 temperature dependence coefficient of P(20), with uncertainties (<6.2%) information being given.

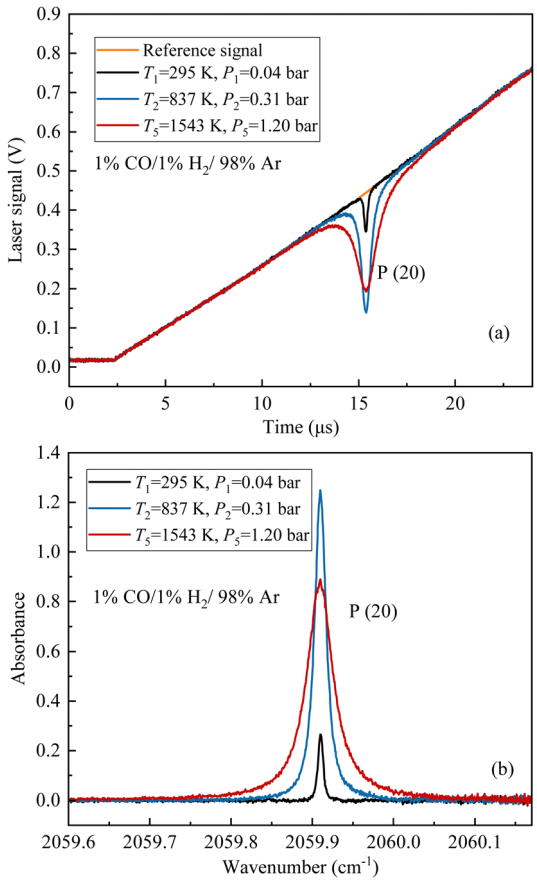

Fig. 8 Laser signal (a) and measured spectra (b) of CO at different status in the shock tube.

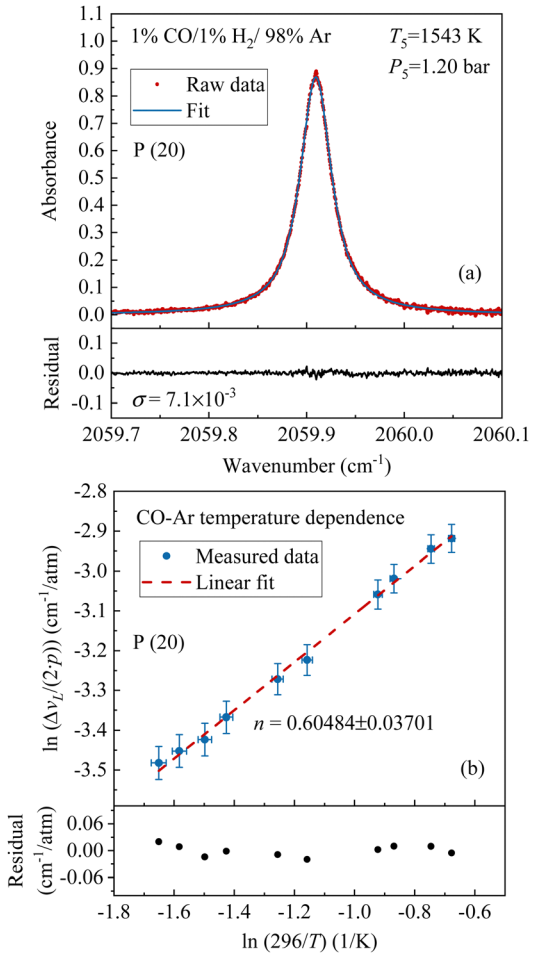

Fig. 9 (a) CO absorption spectra in 1% CO/1% H_2/98% Ar; (b) temperature dependence coefficient of CO–Ar.

4.3 Discussions

In this section, an application was conducted to illustrate the importance of uncertainty of line parameters on CO mole

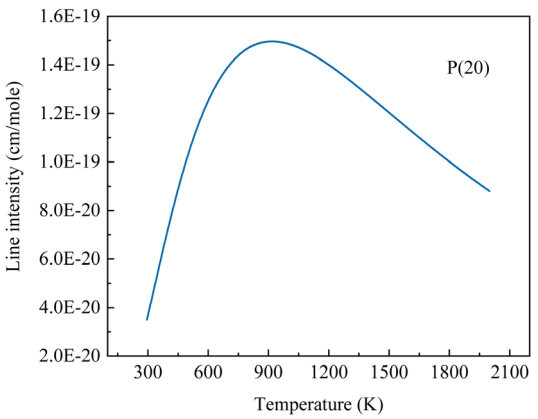

Fig. 10 Variation of line intensity *versus* temperature.

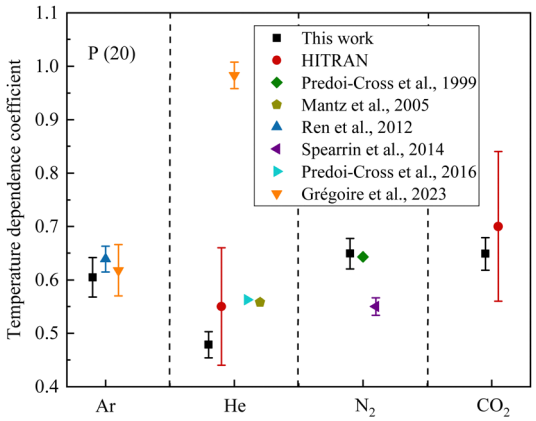

Fig. 11 Comparison of temperature dependency coefficients with literature results.

fraction quantification. The background is toward the combustion kinetic study where accurate speciation profiles are valuable inputs for kinetic mechanism validation. Here high-temperature methane (CH_4) oxidation was taken as a case study where CO mole fraction profile can be used for CH_4 mechanism validation. CH_4 mechanism is vital for optimizing energy production, reducing environmental pollutants, mitigating climate change, ensuring safety, advancing technology, developing alternative fuels, supporting the chemical industry, and improving computational modeling for efficient system design.

To comprehensively evaluate the line parameters, we prepared a mixture of 3.3% CH_4/6.7% O_2/20% He/70% Ar including both buffer gases of He and Ar. Also, 20% He can effectively and sufficiently suppress the vibrational relaxation problem of CO without perturbating the chemical process. To achieve a high time resolution, a fixed-wavelength LAS was used by tunning the P(20) laser at its central wavelength of 2059.91 cm^{-1}.

According to the 'Guide to the expression of uncertainty in measurement (GUM)', the combined standard uncertainty $u(x)$ is the positive squared root of the combined variance which is given by:[38]

$$u(x) = \sqrt{\sum_{i=1}^{N}\left(\frac{\partial f}{\partial Y_i}\cdot u(Y_i)\right)^2} \quad (6)$$

where $u(Y_i)$ is the uncertainty of the i_{th} quantity Y_i.

Table 2 Summary of P(20) temperature dependency coefficients

P(20)	Ar	He	N_2	CO_2
1999, Predoi-Cross *et al.*[24]			0.643	
2005, Mantz *et al.*[26]		0.558		
2012, Ren *et al.*[18]	0.639 (24)			
2014, Spearrin *et al.*[33]			0.550 (17)	
2016, Predoi-Cross *et al.*[29]		0.563		
2023, Grégoire *et al.*[34]	0.618 (48)	0.983 (25)		
HITRAN[32]		0.550 (11)		0.700 (14)
This study	0.605 (37)	0.478 (25)	0.649 (28)	0.649 (30)

The uncertainties are given in parentheses.

For the uncertainty of CO mole fraction, the correlations between mole fraction x and related quantities Y_i can be expressed through a functional relationship:

$$x = f(\alpha(\nu), L, p, T, \nu_0, S, \gamma, n) \quad (7)$$

where L is the optical path length, S is the line intensity. Once the uncertainty of each quantity is clear, the uncertainty of the CO mole fraction can be calculated by eqn (6).

For CO mole fraction calculation using line parameters from HITRAN, there are no data on CO–Ar pressure broadening coefficient (γ_{CO-Ar}) and temperature dependence coefficient (n_{CO-Ar}) available in the HITRAN database. Therefore, the value of CO–air pressure broadening coefficient (γ_{CO-air}) and temperature dependence coefficient (n_{CO-air}) in HITRAN was adopted as replacements and assigned an uncertainty of 20%. Another clarification is the pressure broadening and temperature dependence of the other 10% gases (except 20% He and 70% Ar) which are dynamically changing during the oxidation. This point has been discussed in our previous work[39] and is beyond the scope of this study. Here we simplified to assign $\gamma_{CO\text{-}rest}$ with a fixed value adopting from γ_{CO-air} measured in this study and assign $n_{CO\text{-}rest}$ with a default value of 0.5. Both $\gamma_{CO\text{-}rest}$ and $n_{CO\text{-}rest}$ are assigned with an uncertainty of 20%.

Fig. 12 shows the time-resolved CO mole fraction during the CH_4 oxidation in the shock tube using the pressure broadening coefficients and temperature dependence coefficients measured in this study (red line) and HITRAN database (blue line). On one hand, the difference between both calculated CO mole fractions is relatively small. But it should be careful that the CO profile using line parameters from HITRAN is an 'unreal' value as γ_{CO-Ar} and n_{CO-Ar} are missing and were manually assigned. On the other hand, what matters most is the uncertainty of CO mole fraction indicated by the shadows, which are 2.7 times difference.

As mentioned above, since the HITRAN database does not provide spectroscopy data for Ar and has much higher uncertainties in spectroscopy data for He, it results in significant uncertainty in the overall concentration calculation as

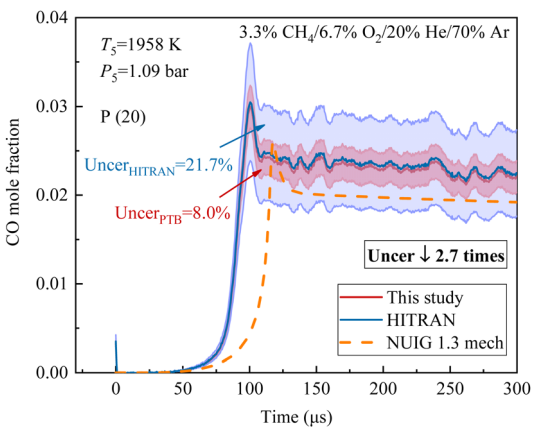

Fig. 12 Time-resolved CO mole fraction of CH_4 oxidation measured in the shock tube and calculated using NUIG 1.3 mechanism.[40]

Table 3 Uncertainty budgets of CO mole fraction

	This study			HITRAN[32]		
Quantity	Value	Uncer (%)	Index (%)	Value	Uncer (%)	Index (%)
$\alpha(v)$	0.7	0.7	0.76	0.7	0.7	0.1
L	7 cm	1.1	1.87	7 cm	1.1	0.26
p	1.7 bar	1.5	0.06	1.7 bar	1.5	0.008
T	2700 K	2.2	38.4	2700 K	2.2	5
v_0	2059.91 cm^{-1}	0.0001	2.87×10^{-9}	2059.91 cm^{-1}	0.0001	4.01×10^{-10}
$S(T_0)$	3.535×10^{-20} cm per molecule	2.5	9.67	3.535×10^{-20} cm per molecule	2.5	1.33
γ_{CO-Ar}	0.03947 cm^{-1} per atm	0.51	0.1	0.051 cm^{-1} per atm	20	26.98
γ_{CO-He}	0.04828 cm^{-1} per atm	0.66	0.038	0.0464 cm^{-1} per atm	10	0.77
$\gamma_{CO-rest}$	0.05159 cm^{-1} per atm	20	8.79	0.05159 cm^{-1} per atm	20	1.17
n_{CO-Ar}	0.60484	6.12	26.95	0.67	20	58.43
n_{CO-He}	0.47844	5.15	2.57	0.55	20	4.52
$n_{CO-rest}$	0.5	20	10.74	0.5	20	1.43
$\boldsymbol{x_{CO}}$	**0.0267**	**8.0**		**0.0272**	**21.7**	

emphasized in the uncertainty budget in Table 3. Thus, this case study has strongly proved the importance of accurate line parameters in reducing the uncertainty of CO mole fraction quantification. Furthermore, we performed kinetic modelling to simulate the CO profile using NUIG 1.3 mechanism,[40] as shown in Fig. 12. The simulated CO mole fraction is within the 21.7% uncertainty range based on HITRAN database, but it is already beyond the range of 8% uncertainty based on the spectroscopy parameters measured in this study. This result indicates that low uncertainty data can provide guidance on the refinement of chemical kinetics models.

5. Conclusions

Accurate quantification of carbon monoxide (CO) is vital as it is a widely utilized molecule across various application scenarios. Considering the strongest line intensities and relatively smaller interferences, four CO transition lines near 4.9 μm in the fundamental band are studied. Two LAS-based spectrometers have been developed to measure pressure broadening coefficients and temperature dependence coefficients, respectively.

For pressure broadening coefficient measurements, one ICL laser centered at 4855 nm was used to study P(20) and another ICL laser centered at 4925 nm was used to study P(27), P(16) and P(26). Both lasers were coupled to a single gas cell. For the first time, pressure broadening coefficients of P(20), P(27), P(16) and P(26) perturbed by Ar, He, H_2, O_2, N_2, CO_2, and air were consistently measured and reported. The pressure broadening coefficient monotonically decreases with the increase of line number $|m|$, namely pressure broadening coefficients decrease from P(16) ($m = -16$) to P(27) ($m = -27$). This tendency is consistent with the literature results. The variation of pressure broadening coefficients at different buffer gases are consistent for all four lines, *e.g.* the CO–H_2 and CO–Ar show the highest and lowest pressure broadening coefficients, respectively. The measured pressure broadening coefficients align with most literature results, but the uncertainties in the current study are significantly lower. For most results, the uncertainty is below 1%.

Secondly, the P(20) laser was coupled into a shock tube for temperature dependence coefficient measurements. With a rapid scan frequency of 20 kHz, for the first time, the spectra between incident shock and reflected shock were also used for temperature dependence coefficient calculations. The novelty is to get more information at two different temperature and pressure combinations within a single shot. On that basis, CO–Ar, CO–He, CO–N_2 and CO–CO_2 temperature dependence coefficients of P(20) were measured with uncertainties below 6.2%. The results are consistent with most literature results.

As a case study, CH_4 oxidation experiments were conducted in the shock tube using a fixed-wavelength LAS for high time resolution. This application case shows the feasibility of using measured line parameters to quantify time-resolved CO profiles. Moreover, the metrological uncertainty analysis reveals that the uncertainty of CO mole fraction can be reduced by a factor of 2.7 using the line parameters measured in this study compared to those from the HITRAN database. Overall, the newly collected data, with minimal uncertainties, greatly improve the spectroscopic database, allowing for more accurate quantification of CO mole fractions in diverse application scenarios.

For future work, we intend to measure temperature dependence coefficients in a heated cell which provides more stable temperature and pressure conditions, to further reduce the uncertainty. Besides, from Table 3, the $\gamma_{CO-rest}$ and $n_{CO-rest}$ contribute 8.79% and 10.74% uncertainties to the CO mole fraction, respectively. We are trying to figure out the uncertainties brought by those'rest' buffer gases.

Author contributions

Denghao Zhu: investigation, visualization, writing – original draft; Leopold Seifert: investigation, writing – review and editing; Sumit Agarwal: investigation, writing – review and editing; Bo Shu: writing – review and editing; Ravi Fernandes: writing – review and editing; Zhechao Qu: investigation, writing – review and editing, funding acquisition.

Data availability

Data are available upon request from the authors.

Conflicts of interest

There are no conflicts to declare.

Acknowledgements

The project (22IEM03 PriSpecTemp) has received funding from the European Partnership on Metrology, co-financed from the European Union's Horizon Europe Research and Innovation Programme and by the Participating States.

References

1 J. Falbe, *Carbon monoxide in organic synthesis*, Springer Science & Business Media, 2013.
2 M. A. Vannice, The catalytic synthesis of hydrocarbons from carbon monoxide and hydrogen catalysis reviews: science and engineering, *Catal. Rev.:Sci. Eng.*, 1976, **14**, 153–191.
3 J. C. McConnell, M. B. McElroy and S. C. Wofsy, Natural sources of atmospheric CO, *Nature*, 1971, **233**(5316), 187–188.
4 B. Weinstock and H. Niki, Carbon Monoxide Balance in Nature, *Science*, 1972, **176**(4032), 290–292.
5 T. Holloway, H. Levy and P. Kasibhatla, Global distribution of carbon monoxide, *J. Geophys. Res.: Atmos.*, 2000, **105**, 12123–12147.
6 L. J. Rickard, P. Palmer, M. Morris, B. Zuckerman and B. E. Turner, Detection of extragalactic carbon monoxide at millimeter wavelengths, *Astrophys. J.*, 1975, **99**, L75–L78.
7 T. M. Bania, Carbon monoxide in the inner Galaxy, *Astrophys. J.*, 1977, **216**, 381–403.
8 H. S. Liszt and W. B. Burton, The gas distribution in the central region of the Galaxy. II-Carbon monoxide, *Astrophys. J.*, 1978, **226**, 790–816.
9 J. B. Howard, G. C. Williams and D. H. Fine, Kinetics of carbon monoxide oxidation in postflame gases, *Symp. Combust. Proc.*, 1973, **14**(1), 975–986.
10 C. T. Bowman, Kinetics of pollutant formation and destruction in combustion, *Prog. Energy Combust. Sci.*, 1975, **1**(1), 33–45.
11 R. A. Yetter, F. L. Dryer and H. Rabitz, A Comprehensive Reaction Mechanism For Carbon Monoxide/Hydrogen/Oxygen Kinetics, *Combust. Sci. Technol.*, 1991, **79**, 97–128.
12 W. K. Cheung, Y. Zeng, S. Lin and X. Huang, Modelling carbon monoxide transport and hazard from smouldering for building fire safety design analysis, *Fire Saf. J.*, 2023, **140**, 103895.
13 J. Li, U. Parchatka and H. Fischer, Development of field-deployable QCL sensor for simultaneous detection of ambient N_2O and CO, *Sens. Actuators, B*, 2013, **182**, 659–667.
14 D. Zhu, L. Seifert, S. Agarwal, B. Shu, R. Fernandes and Z. Qu, NH_3 line broadening coefficients and intensities measurement and impurities determination in emerging applications: CCUS, Biomethane and H_2, *Spectrochim. Acta, Part A*, 2024, **320**, 124642.
15 X. Yang, Z. Zhang, H. Xia, P. Sun, T. Pang, B. Wu, X. Liu and Q. Guo, Re-injection off-axis integrated cavity output spectroscopy for the simultaneous detection of N_2O, H_2O and CO with a mid-infrared QCL laser, *Analyst*, 2024, **149**, 909–916.
16 J. Li, H. Deng, J. Sun, B. Yu and H. Fischer, Simultaneous atmospheric CO, N_2O and H_2O detection using a single quantum cascade laser sensor based on dual-spectroscopy techniques, *Sens. Actuators, B*, 2016, **231**, 723–732.
17 Q. Huang, Y. Wei and J. Li, Simultaneous detection of multiple gases using multi-resonance photoacoustic spectroscopy, *Sens. Actuators, B*, 2022, **369**, 132234.
18 W. Ren, A. Farooq, D. F. Davidson and R. K. Hanson, CO concentration and temperature sensor for combustion gases using quantum-cascade laser absorption near 4.7 μm, *Appl. Phys. B*, 2012, **107**, 849–860.
19 C. Crane-Robinson and H. W. Thompson, Pressure broadening studies on vibration-rotation bands, IV. Optical collision diameters for foreign-gas broadening of CO and DCl bands, *Proc. R. Soc. London, Ser. A*, 1963, **272**, 453–466.
20 J.-P. Bouanich and C. Haeusler, Linewidths of carbon monoxide self-broadening and broadened by argon and nitrogen, *J. Quant. Spectrosc. Radiat. Transfer*, 1972, **12**, 695–702.
21 P. L. Varghese and R. K. Hanson, Tunable infrared diode laser measurements of line strengths and collision widths of $^{12}C^{16}O$ at room temperature, *J. Quant. Spectrosc. Radiat. Transfer*, 1980, **24**, 479–489.
22 F. Thibault, J. Boissoles, R. Le Doucen, R. Farrenq, M. Morillon-Chapey and C. Boulet, Line-by-line measurements of interference parameters for the 0–1 and 0–2 bands of CO in He, and comparison with coupled-states calculations, *J. Chem. Phys.*, 1992, **97**, 4623–4632.
23 P. M. Sinclair, P. Duggan, R. Berman, J. R. Drummond and A. D. May, Line Broadening in the Fundamental Band of CO in CO–He and CO–Ar Mixtures, *J. Mol. Spectrosc.*, 1998, **191**, 258–264.
24 A. Predoi-Cross, C. Luo, P. M. Sinclair, J. R. Drummond and A. D. May, Theoretical and revisited experimentally retrieved He-broadened line parameters of carbon monoxide in the fundamental band, *J. Mol. Spectrosc.*, 1999, **198**, 291–303.
25 Q. Zou and P. Varanasi, New laboratory data on the spectral line parameters in the 1-0 and 2-0 bands of $^{12}C^{16}O$ relevant to atmospheric remote sensing, *J. Quant. Spectrosc. Radiat. Transfer*, 2002, **75**, 63–92.
26 A. W. Mantz, V. M. Devi, D. Chris Benner, M. A. H. Smith, A. Predoi-Cross and M. Dulick, A multispectrum analysis of widths and shifts in the 2010–2260 cm^{-1} region of $^{12}C^{16}O$ broadened by Helium at temperatures between 80 and 297 K, *J. Mol. Struct.*, 2005, **742**, 99–110.
27 L. Régalia-Jarlot, X. Thomas, P. Von der Heyden and A. Barbe, Pressure-broadened line widths and pressure-induced line shifts coefficients of the (1-0) and (2-0) bands of $^{12}C^{16}O$, *J. Quant. Spectrosc. Radiat. Transfer*, 2005, **91**, 121–131.
28 K. Sung and P. Varanasi, CO_2-broadened half-widths and CO_2-induced line shifts of $^{12}C^{16}O$ relevant to the atmospheric spectra of Venus and Mars, *J. Quant. Spectrosc. Radiat. Transfer*, 2005, **91**, 319–332.

29 A. Predoi-Cross, K. Esteki, H. Rozario, H. Naseri, S. Latif, F. Thibault, V. M. Devi, M. A. H. Smith and A. W. Mantz, Theoretical and revisited experimentally retrieved He-broadened line parameters of carbon monoxide in the fundamental band, *J. Quant. Spectrosc. Radiat. Transfer*, 2016, **184**, 322–340.

30 V. M. Devi, D. C. Benner, K. Sung, T. J. Crawford, G. Li, R. R. Gamache, M. A. H. Smith, I. E. Gordon and A. W. Mantz, Positions, intensities and line shape parameters for the $1 \leftarrow 0$ bands of CO isotopologues, *J. Quant. Spectrosc. Radiat. Transfer*, 2018, **218**, 203–230.

31 R. Hashemi, I. E. Gordon, E. M. Adkins, J. T. Hodges, D. A. Long, M. Birk, J. Loos, C. D. Boone, A. J. Fleisher, A. Predoi-Cross and L. S. Rothman, Improvement of the spectroscopic parameters of the air- and self-broadened N_2O and CO lines for the HITRAN2020 database applications, *J. Quant. Spectrosc. Radiat. Transfer*, 2021, **271**, 107735.

32 I. E. Gordon, L. S. Rothman, R. J. Hargreaves, R. Hashemi, E. V. Karlovets, F. M. Skinner, E. K. Conway, C. Hill, R. V. Kochanov and Y. Tan, *et al.*, The HITRAN2020 molecular spectroscopic database, *J. Quant. Spectrosc. Radiat. Transfer*, 2022, **277**, 107949.

33 R. M. Spearrin, C. S. Goldenstein, J. B. Jeffries and R. K. Hanson, Quantum cascade laser absorption sensor for carbon monoxide in high-pressure gases using wavelength modulation spectroscopy, *Appl. Opt.*, 2014, **53**, 1938–1946.

34 C. M. Grégoire, O. Mathieu and E. L. Petersen, High-temperature line strengths with He and Ar broadening coefficients of the P(20) line in the $1 \leftarrow 0$ band of carbon monoxide, *Appl. Phys. B*, 2023, **129**, 187.

35 D. Zhu, Z. Qu, M. Li, S. Agarwal, R. Fernandes and B. Shu, Investigation on the NO formation of ammonia oxidation in a shock tube applying tunable diode laser absorption spectroscopy, *Combust. Flame*, 2022, **246**, 112389.

36 D. Zhu, S. Agarwal, L. Seifert, B. Shu, R. Fernandes and Z. Qu, NH_3 absorption line study and application near 1084.6 cm^{-1}, *Infrared Phys. Technol.*, 2024, **136**, 105058.

37 D. Zhu, S. Agarwal, B. Shu, R. Fernandes and Z. Qu, An ultra-rapid optical gas standard for dynamic processes: Absolute NH_3 quantification and uncertainty evaluation, *Measurement*, 2024, **230**, 114559.

38 JCGM 100:2008, *Evaluation of measurement data—Guide to the expression of uncertainty in measurement*, 2008.

39 M. Li, D. Zhu, H. Karas, S. Agarwal, Z. Qu, K. Moshammer, R. Fernandes and B. Shu, NH_3/C_2H_6 and NH_3/C_2H_5OH oxidation in a shock tube: Multi-speciation measurement, uncertainty analysis, and kinetic modeling, *Chem. Eng. J.*, 2024, **498**, 155041.

40 S. Dong, B. Wang, Z. Jiang, X. Cheng, B. Liu, H. Wang, Z. Wang, C. Zhou and H. J. Curran, On the low-temperature chemistry of 1,3-butadiene, *Proc. Combust. Inst.*, 2023, **39**(1), 365–373.